The Astrophysical Journal, 772:82 (13pp), 2013 August 1 doi:10.1088/0004-637X/772/2/82

A CATALOG OF GLOBULAR CLUSTER SYSTEMS: WHAT DETERMINES THE SIZE OF A GALAXY'S GLOBULAR CLUSTER POPULATION?

William E. Harris[1], Gretchen L. H. Harris[2], and Matthew Alessi[1]
[1] Department of Physics and Astronomy, McMaster University, Hamilton, ON L8S 4M1, Canada; harris@physics.mcmaster.ca, alessimj@mcmaster.ca
[2] Department of Physics and Astronomy, University of Waterloo, Waterloo, ON N2L 3G1, Canada; glharris@astro.uwaterloo.ca
Received 2013 January 8; accepted 2013 May 24; published 2013 July 9

ABSTRACT

We present a catalog of 422 galaxies with published measurements of their globular cluster (GC) populations. Of these, 248 are E galaxies, 93 are S0 galaxies, and 81 are spirals or irregulars. Among various correlations of the total number of GCs with other global galaxy properties, we find that $N_{\rm GC}$ correlates well though nonlinearly with the dynamical mass of the galaxy bulge $M_{\rm dyn} = 4\sigma_e^2 R_e/G$, where σ_e is the central velocity dispersion and R_e the effective radius of the galaxy light profile. We also present updated versions of the GC specific frequency S_N and specific mass S_M versus host galaxy luminosity and baryonic mass. These graphs exhibit the previously known U-shape: highest S_N or S_M values occur for either dwarfs or supergiants, but in the midrange of galaxy size (10^9–$10^{10}\,L_\odot$) the GC numbers fall along a well-defined baseline value of $S_N \simeq 1$ or $S_M = 0.1$, similar among all galaxy types. Along with other recent discussions, we suggest that this trend may represent the effects of feedback, which systematically inhibited early star formation at either very low or very high galaxy mass, but which had its minimum effect for intermediate masses. Our results strongly reinforce recent proposals that GC formation efficiency appears to be most nearly proportional to the galaxy halo mass $M_{\rm halo}$. The mean "absolute" efficiency ratio for GC formation that we derive from the catalog data is $M_{\rm GCS}/M_{\rm halo} = 6 \times 10^{-5}$. We suggest that the galaxy-to-galaxy scatter around this mean value may arise in part because of differences in the relative timing of GC formation versus field-star formation. Finally, we find that an excellent empirical predictor of total GC population for galaxies of all luminosities is $N_{\rm GC} \sim (R_e\sigma_e)^{1.3}$, a result consistent with fundamental plane scaling relations.

Key words: galaxies: general – galaxies: star clusters: general – globular clusters: general

Online-only material: color figures, machine-readable table

1. INTRODUCTION

A globular cluster system (GCS) is the ensemble of all such star clusters within a given galaxy. The history of GCS studies in the astronomical literature can properly be said to begin with Shapley's (1918) work on the Milky Way GCS, which he used to make the first reliable estimate of the distance to the Galactic center. Next pioneering steps were taken with reconnaissance of the M31 GCS (Hubble 1932; Kron & Mayall 1960; Vetesnik 1962, among others) and the other Local Group galaxies (see Harris & Racine 1979; Harris 1991 for reviews of this early history). However, it was not until discovery and measurement of the rich GC populations around the Virgo elliptical galaxies had begun (Baum 1955; Sandage 1968; Racine 1968; Hanes 1977; Harris & Smith 1976; Strom et al. 1981) that GCS studies began to emerge as a distinct field.

It is now realized that virtually all galaxies more luminous than $\sim 3 \times 10^6\,L_\odot$ (that is, all but the tiniest dwarfs) contain old globular clusters (GCs), and that these massive, compact star clusters represent a common thread in the earliest star formation history in every type of galaxy. The first "catalog" of GCSs (Harris & Racine 1979) listed just 27 galaxies, all from either the Local Group or the Virgo Cluster. By 1991 the number had grown to 60 (Harris 1991) and a decade later to 73 (Harris & Harris 2000), with the sample starting to include galaxies in a wider range of environments. Other compilations for different purposes were put together by Brodie & Strader (2006), Peng et al. (2008), Spitler et al. (2008), and Georgiev et al. (2010).

In the past decade, many new surveys of GCSs for galaxies throughout the nearby universe have taken place. The relevance of GCS properties to understanding galactic structure and early evolution is becoming increasingly apparent, so the construction of a complete new catalog is well justified. A new list may reveal large-scale trends of GCS properties with galaxy type or environment, and may also provide a springboard for designing new studies. Perhaps the most basic question, and one that dates back decades, is simply to ask what determines the total population of GCs in a galaxy. The total GC population size, $N_{\rm GC}$, must relate to the GC formation efficiency relative to the field-star population as well as to the later dynamical evolution of the system. In this paper, we address these questions by using a newly constructed GCS catalog to search for correlations of cluster population size with several other global properties of their host galaxies.

2. THE DATA SAMPLE AND A GCS CATALOG

We have carried out an extensive literature search to find published studies of galaxies that, at a minimum, give some useful, quantitative information for the total number $N_{\rm GC}$ of its GCs. Much of this material now comes from a few recent major surveys that have the distinct advantage of being internally homogeneous, such as for the Virgo Cluster galaxies (Peng et al. 2006), the Fornax Cluster (Villegas et al. 2010), nearby dwarf galaxies (Lotz et al. 2004; Georgiev et al. 2008, 2009), nearby E and S0 galaxies (Kundu & Whitmore 2001a, 2001b; Larsen et al. 2001), and supergiant E galaxies (Blakeslee 1997, 1999; Harris et al. 2006; Harris 2009). The *Hubble Space Telescope* (*HST*) cameras including WFPC2, Advanced Camera for Surveys, and

Table 1
Globular Cluster Systems

Galaxy	α	δ	Type	D (Mpc)	$\pm$	A_V	M_V^T	$\pm$	M_K	$\pm$	N_{GC}	$\pm$	σ_e (km s^{-1})	$\pm$	R_e (kpc)	$\pm$	$\log(M_{GCS}/M_\odot)$
NGC 55	0.2482245	−39.1965824	SBm	2.09	0.08	0.036	−18.770	0.20	−20.356	0.111	36.0	15.0			2.31	0.09	6.87
NGC 147	0.553330	+48.50860	E5	0.76	0.10	0.475	−15.460	0.30	−17.254	0.118	7.0	2.0	22.0	5.00	0.57	0.08	6.01
NGC 185	0.6493737	+48.3373957	E3	0.63	0.01	0.50	−15.40	0.20	−17.489	0.112	8.0	1.0	19.9	2.4	0.35	0.04	6.07

Note. The complete catalog with references is available at http://physwww.mcmaster.ca/~harris/Databases.html.

(This table is available in its entirety in a machine-readable form in the online journal. A portion is shown here for guidance regarding its form and content.)

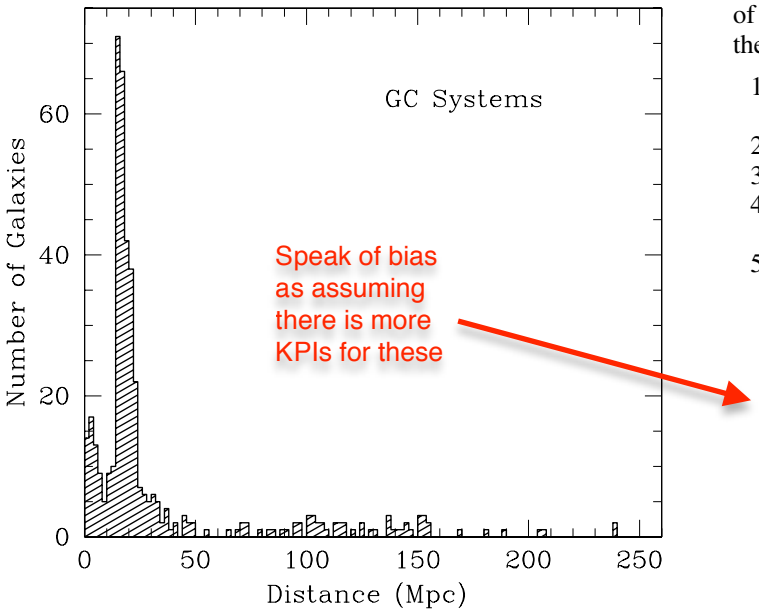

Figure 1. Distribution by distance of the 417 galaxies in Table 1. For comparison, the Virgo Cluster is at $D = 16$ Mpc and the Coma Cluster at $D = 100$ Mpc.

most recently WFC3 have provided a powerful stimulus for the imaging and photometry that such surveys depend on.

However, dozens of other GCS studies exist that are widely scattered through the literature, and we have searched thoroughly for these as well. In total we have extracted GCS data from 112 papers published up to 2012 December. These yield N_{GC} measurements for 422 individual galaxies, a dramatic increase over previous compilations.

The distribution by distance for the galaxies in the catalog is shown in Figure 1. Here, the predominance of targets in the Virgo-to-Fornax distance range (15–25 Mpc) is obvious, but the numbers of more remote galaxies are gradually increasing as new work goes on. In general, the *HST* cameras can reach GCSs reliably for $D \lesssim 200$ Mpc (about twice the Coma Cluster distance), the necessary exposure times becoming quite large beyond that (cf. Harris et al. 2006). By comparison, GCS measurement through ground-based imaging becomes difficult for $D \gtrsim 40$ Mpc even with 8 m class telescopes, an empirical limit that partly determines the steep dropoff of targets beyond that distance.

A sample of the data in our new catalog is shown in Table 1. The complete catalog with literature sources can be obtained from the Web site of the first author at http://physwww.mcmaster.ca/~harris/Databases.html.

In addition to N_{GC}, we include some selected observational parameters describing the luminosities, masses, and scale sizes of the galaxies and that are available for most of the objects in the list. The full catalog contains the following information.

1. Galaxy identification (from more than one catalog source if appropriate).
2. Right ascension and declination (J2000).
3. Morphological type.
4. Foreground absorption A_V, from NED (NASA/IPAC Extragalactic Database).
5. Distance D, primarily from the raw data in NED. For relatively nearby galaxies, wherever possible we adopt D-values measured from primary standard candles based on resolved stellar populations (Cepheids, red-giant-branch-tip stars, planetary nebula luminosity functions, Mira stars, RR Lyrae stars). Surface brightness fluctuations measured from integrated light are also used as a standard candle. For each such galaxy we adopt the average of the most recent individual measurements of those six primary methods (we emphasize that our adopted values are *not* the averages given in NED). For some slightly more distant galaxies for which these primary indicators are not available, we use recent determinations from the Tully–Fisher relation as listed in NED. For still more distant systems ($D \gtrsim 30$ Mpc) we use Hubble's law with $H_0 = 70$ km s^{-1} Mpc^{-1} and with the galaxy radial velocity corrected to the cosmic microwave background reference frame.
6. Absolute visual magnitude M_V^T, calculated from the distance modulus and the integrated magnitude V_T^0 if available from NED. In other cases where a total V magnitude was unavailable we have used a blue magnitude B^T and integrated $(B - V)$ color taken from the HyperLeda database.
7. Absolute near-infrared (near-IR) magnitude M_K^T, calculated from the distance modulus and the integrated K magnitude from Two Micron All Sky Survey (2MASS). We use here the 2MASS K(ext) magnitude for each galaxy, a quantity which is available for 82% of the galaxies in our catalog. Although an alternate and perhaps preferable choice would be the frequently used K_s band, this is unavailable for most of our galaxies.
8. Total number of GCs in the galaxy, N_{GC}.
9. Stellar velocity dispersion σ_e. This spectroscopic quantity is dominated by the bright inner part of the galaxy and in most cases represents the velocity dispersion of the bulge light. Where possible we have taken the homogeneous σ_e values given by Gultekin et al. (2009), McElroy (1995), and McConnell et al. (2012). Otherwise, we use σ_e as compiled in HyperLeda. In total, σ_e measurements are available for 65% of the galaxies in the catalog.
10. Effective radius R_e enclosing half the total galaxy light, taken from NED or (secondarily) HyperLeda. Here, in the interests of the best possible combination of homogeneity and completeness, we use only radii measured through

optical photometry: primarily V whenever available, and secondarily other nearby bands, including g, r, or B. We do not use any values measured through infrared or near-ultraviolet bands, since these give systematically different R_e from optical bandpasses. In total, optically based R_e values are available for 81% of the galaxies.

11. Dynamical mass $M_{\rm dyn}$ of the galaxy, calculated from σ_e and R_e as described in Section 3 below.
12. Total stellar mass $M_{\rm GCS}$ contained in the entire GC population of the galaxy, calculated as described below in Section 3.3.
13. Measured mass of the central supermassive black hole (SMBH), a quantity of special interest although it is currently available for only 11% of the galaxies in our GCS list. SMBH data are taken from Gultekin et al. (2009), McConnell et al. (2012), Graham (2008), and other sources listed in Harris & Harris (2011) and Harris et al. (2013).

Comments.

1. The only quantities available for *all* the galaxies in the catalog are $N_{\rm GC}$, galaxy type, and luminosity M_V^T. In principle, a total magnitude obtained from a near-IR band such as z, I, or K is a better photometric proxy for total stellar *mass* than are optical bands. Internally homogeneous near-IR luminosities are available for subsets of the data (for example, the Virgo and Fornax Cluster surveys; see Peng et al. 2008; Villegas et al. 2010, hereafter P08, V10), but at present we place most of our reliance on absolute visual magnitudes because these are available for all of the targets, and allow us to compare various results readily with earlier work. In the discussion below, we also present some correlations with M_K from the 2MASS K(ext) data, but these generally do not exhibit any smaller scatter than the ones using M_V^T.
2. The velocity dispersion σ_e is a key quantity in many studies of the "fundamental plane" (FP) of early-type galaxies (e.g., Djorgovski & Davis 1987; Allanson et al. 2009; Graves & Faber 2012, among many others). It is a critical element to dynamical estimates of galaxy mass (see below), and is a valuable indicator of the depth of the galaxy's potential well (Loeb & Peebles 2003; Shankar et al. 2006). An additional advantage to including σ_e here is that it appears to be stable with time for early-type galaxies over a significant range of redshift, as would be the case if large galaxies form their major core light at high redshift and then evolve later by inside-out growth mainly through minor mergers (Bezanson et al. 2009, 2011; Tiret et al. 2011; Patel et al. 2013). The scale radius R_e, by contrast, is expected to grow with time (e.g., Papovich et al. 2012; Shankar et al. 2013).
3. The population size $N_{\rm GC}$ is only a simple first-order gauge of a GCS. Other GCS characteristics that are of strong interest include the GCS *radial profile*, the GC *luminosity distribution* (GCLF), and the *metallicity distribution* (MDF). The MDF in particular—in most cases measured through broad-band color indices—has stimulated much ongoing discussion of the cluster formation process (e.g., Ashman & Zepf 1992; Larsen et al. 2001; Peng et al. 2006; Harris 2009; Spitler et al. 2008; Mieske et al. 2010, among many others). Many of the sources listed in our bibliography discuss these other characteristics, but a comprehensive analysis of them extends far beyond the goals of our present study. For each galaxy we have selected the studies that gave the best estimates of the total GC population, not necessarily the best analysis of the MDF or other characteristics.
4. It should be emphasized that the $N_{\rm GC}$ values collected here are of greatly differing internal uncertainty from one galaxy to the next and thus certainly do not make up a homogeneous list. Ideally, $N_{\rm GC}$ should be determined from imaging that is both deep enough to reach nearly to the faint limit of the GCLF and also wide-field enough to cover the full radial extent of the GCS, as well as to determine the background contamination level accurately. These twin conditions are rarely met. The most commonly used technique is to obtain GC photometry with a limiting magnitude near the "turnover" or peak point of the GCLF and then fit a standard Gaussian GCLF shape to predict the total over all magnitudes. If (as is usually the case) the field coverage does not sample the entire halo of the target galaxy, then some outward extrapolation of the GCS radial profile beyond the heavily populated inner regions is also needed to estimate the total over all galactocentric radii. Good recent examples of the standard techniques can be found, for example, in Jordán et al. (2007), P08, Young et al. (2012), and references cited there. In all cases the GC population totals are simply the best attempts, with the available imaging data, to extrapolate over the full luminosity range and spatial range needed. Inspection of Table 1 will show that the quoted relative uncertainties $\Delta(N_{\rm GC})/N_{\rm GC}$ span a wide range: at best the population total is known to $\pm 10\%$ while at worst it may be uncertain by as much as a factor of two. We return to this point in the later discussion.
5. Earlier GCS lists were dominated by large E galaxies with rich GC populations. The current catalog now reduces many sampling biases: it includes the complete range of galaxy environment, type, and luminosity, from the smallest dwarfs to the largest supergiants. Our catalog contains 248 ellipticals, 93 S0s, and 81 spirals or irregulars. The smallest one in the list is the dSph KKS-55 at $M_V^T = -11.2$ holding a single GC, while the largest are cD/BCG supergiants with $M_V^T \simeq -24$ and holding up to 30,000 GCs each.
6. We note that for most galaxies in this catalog, we have used the single literature source that gives the best recent estimate of the total GC population. This may not correspond to the best sources for other purposes, such as discussions of the MDF. In some cases we have averaged the results from two or more sources that appear to give comparably good estimates of $N_{\rm GC}$. Lastly, in the catalog we have chosen *not* to list any galaxies for which the estimated $N_{\rm GC}$ was zero or negative. Such cases include a few very small dwarfs (Peng et al. 2008; Georgiev et al. 2010) for which $N_{\rm GC} \leqslant 0$ after subtraction of field contamination; or a few galaxies for which the imaging data simply did not reach deep enough to provide a sensible estimate of GC numbers (Kundu & Whitmore 2001a, 2001b). An exception is the Local Group elliptical M32, which we include for historical reasons though it has no clearly identified clusters.

3. CORRELATIONS

Using the entire database, we next explore some simple correlations of $N_{\rm GC}$ with large-scale host galaxy properties such as luminosity, dynamical mass, or scale size. The overall purpose is to use this new and larger data set to search for *reliable predictors of GC population size* that can be calculated from the shortlist of simple structural parameters that are available for most of the galaxies. In doing so, we concentrate particularly on the ellipticals in the catalog, for two reasons: (1) they

cover the largest range in luminosity, from dwarf-spheroidal up to cD supergiants; and (2) they form the largest and most homogeneous subset of the GC measurements, making up almost 60% of the entire catalog.

In general we take pairs of parameters (x, y) in log/log space and search for linear correlations of the normal form $y = \alpha + \beta x$. Assume that we have a sample of n measured datapoints (x_i, y_i) with quoted measurement uncertainties $(\sigma_{xi}, \sigma_{yi})$. Our best-fit slope and zero point are determined by minimizing the sum

$$\chi^2 = \sum_{i=1}^{n} \frac{(y_i - \alpha - \beta(x_i - x_0))^2}{\left(\sigma_{yi}^2 + \epsilon_y^2\right) + \beta^2\left(\sigma_{xi}^2 + \epsilon_x^2\right)} \quad (1)$$

as in Tremaine et al. (2002) and particularly Novak et al. (2006). Here x_0 is a suitable mean value over the sample such that $\langle x - x_0 \rangle \simeq 0$ to minimize the covariance between (α, β).

The parameters (ϵ_x, ϵ_y) are constants that represent any additional variances in (x, y). These variances might be due to intrinsic ("cosmic") scatter built in to the sample population, or extra measurement uncertainties if the quoted (σ_x, σ_y) are underestimated, or a combination of both effects. With only two pairs of measurements (x_i, y_i) in the solution, and without any other external constraints, in general it will not be possible to solve independently for both of ϵ_x, ϵ_y. Therefore in practice for each solution described below, we set $\epsilon_x = 0$ and vary ϵ_y until χ_ν^2, the reduced χ^2 per degree of freedom, equals 1. In the discussion below we refer to ϵ_y determined from the solution as the *residual dispersion* for the dependent variable y (see Novak et al. 2006).

To set up several of the correlation solutions discussed later, we also calculate (1) the total visual luminosity $L_V = 10^{0.4(M_{V\odot} - M_V^T)}\, L_{V\odot}$ with solar $M_{V\odot} = 4.83$; and (2) the dynamical mass,

$$M_{\rm dyn} = \frac{4 R_e \sigma_e^2}{G} \quad (2)$$

following Wolf et al. (2010). Since the luminosity-weighted velocity dispersion is dominated by light from within R_e, and the dark-matter halo contributes a small fraction of the mass within R_e, $M_{\rm dyn}$ is close to being the baryonic mass of the galactic bulge (e.g., Tiret et al. 2011; Graves & Faber 2012). The dynamical mass can be calculated for 61% of the galaxies in our catalog, i.e., the ones with measurements of both σ_e and R_e.

As a preliminary step and a check of our procedures, we show in Figure 2 the direct correlation between $M_{\rm dyn}$ and visual luminosity L_V. The data are shown separately for the E, S0, and spiral galaxies (note that no dwarf irregulars are present here, since they lack any "bulges" from which a velocity dispersion can be measured). It is worth emphasizing that L_V and $M_{\rm dyn}$ are observationally nearly independent measurements except insofar as R_e relies on knowing the large-scale light profile of the galaxy. For the E galaxies over their entire range, the best-fit linear solution is listed in Table 2, along with the other correlations to be presented below. In the table, the successive columns give (1) the pair of parameters (x, y) being fit, (2) the subsample of galaxy types used in the solution, (3) the number of galaxies in the solution, (4–6) the sample mean x_0, zero point α, and slope β, (7) the best-fit residual dispersion ϵ_y, and (8) total rms scatter σ_y of the datapoints around the fitted solution. Throughout Table 2, the luminosities L_V and masses $M_{\rm dyn}$ are in solar units.

The result $M_{\rm dyn} \sim L_V^{1.2}$ corresponds to the well-known systematic increase in mass-to-light ratio with galaxy size

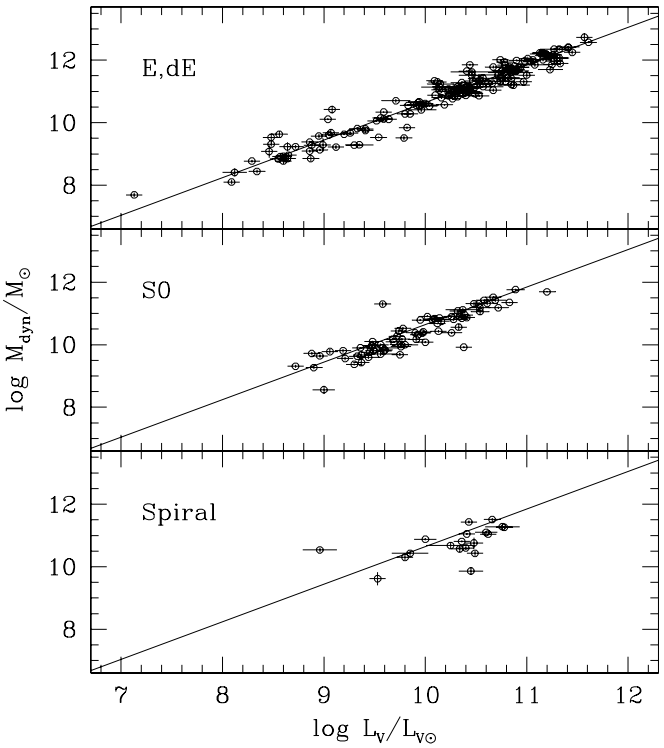

Figure 2. "Dynamical mass" $M_{\rm dyn} = 4R_e\sigma_e^2/G$ plotted vs. total visual luminosity L_V for the galaxies in the GCS catalog. Results are shown separately for the E/dE, S0, and spiral types. In each panel the diagonal line shows the best-fit linear solution to the ellipticals, as described in the text.

derived from the FP of early-type galaxies (e.g., Faber et al. 1987; Jorgensen et al. 1996; Cappellari et al. 2006; Allanson et al. 2009; Magoulas et al. 2012; Graves & Faber 2012). Quantitatively, our E galaxy solution corresponds to

$$(M/L)_V = 4.406(L_V/10^{10}\, L_{V\odot})^{0.2}. \quad (3)$$

The same slope also matches the S0 and spiral-galaxy trends (lower two panels of Figure 2), although these disk galaxies fall below the E line by 0.2–0.3 dex in mass (or alternately, they lie at higher luminosity for a given mass by the same average factor). We use the same mass calculation formula (Equation (2)) for all types, though it is not entirely clear that pure-spheroid (elliptical) systems and disk systems should behave identically or should have the same M/L. The measured scatter of ± 0.27 dex rms in log $M_{\rm dyn}$ about the best-fit line is also encouragingly small, given that the luminosity and calculated mass are derived from a wide variety of observational sources for V^T, σ_e, and R_e and are unavoidably a somewhat heterogeneous sample. As will be seen below, we find very similar scatters for most of our other correlations. In Figure 3, we show all galaxy types together where an offset of 0.2 dex to the calculated mass has been applied to the S0 systems to bring them in line with the ellipticals, and an offset of 0.3 dex to the S/Irr systems.

In Figure 4 we show a similar correlation for the K-band luminosity versus $M_{\rm dyn}$. Plotting the three types of galaxies (E, S0, S/Irr) separately indicates little or no zero point difference, so we show all three combined without offsets. Here we adopt $(\log L_K/L_{K\odot}) = 0.4(3.33 - M_K)$. The best-fit solution over all luminosities (Table 2) gives $M_{\rm dyn} \sim L_K^{1.085\pm0.020}$ and

Table 2
Correlation Solutions

(x, y)	Galaxy Type	N(Sample)	Mean x_0	Zero point α	Slope β	Residual Dispersion ϵ_y	rms Scatter σ_y
$(\log L_V, \log M_{\rm dyn})$	All Ellipticals	161	10.2	10.844 ± 0.021	1.200 ± 0.021	0.24	0.27
$(\log L_K, \log M_{\rm dyn})$	All	238	10.7	10.786 ± 0.017	1.085 ± 0.020	0.255	0.265
	$M_K < -22.4$	174	11.1	11.212 ± 0.019	1.260 ± 0.048	0.240	0.250
	$M_K > -22.4$	67	9.5	9.531 ± 0.033	0.765 ± 0.060	0.26	0.268
$(\log M_{\rm dyn}, \log N_{\rm GC})$	Luminous Es	139	11.2	2.924 ± 0.028	1.035 ± 0.033	0.28	0.32
	Dwarf Es	35	9.2	1.274 ± 0.045	0.365 ± 0.091	0.24	0.27
$(\log E_b, \log N_{\rm GC})$	Luminous Es	129	16.0	3.075 ± 0.027	0.735 ± 0.028	0.29	0.31
$(\log R_e\sigma_e, \log N_{\rm GC})$	All Ellipticals	158	0.20	2.776 ± 0.025	1.290 ± 0.033	0.29	0.32
$(\log R_e, \log N_{\rm GC})$	S/Irr	60	0.4	1.582 ± 0.069	0.995 ± 0.107	0.50	0.53
$(\log M_{\rm dyn}, \log M_{\rm GCS})$	Luminous Es	125	11.4	8.625 ± 0.028	1.160 ± 0.044	0.29	0.31
	Dwarf Es	36	9.2	6.524 ± 0.046	0.460 ± 0.097	0.25	0.27
$(\log L_V, \log R_e)$	Luminous Es	136	10.5	0.648 ± 0.018	0.660 ± 0.029	0.20	0.21
	Dwarf Es	61	8.5	0.020 ± 0.026	0.255 ± 0.054	0.20	0.21
$(\log L_V, \log \sigma_e)$	Luminous Es	142	10.5	2.310 ± 0.009	0.285 ± 0.017	0.09	0.11
	Dwarf Es	36	8.7	1.566 ± 0.025	0.315 ± 0.058	0.14	0.15
$(\log M_{\rm dyn}, \log \langle M_{\rm GC} \rangle)$	All	242	10.7	5.402 ± 0.006	0.098 ± 0.009	0.028	0.086

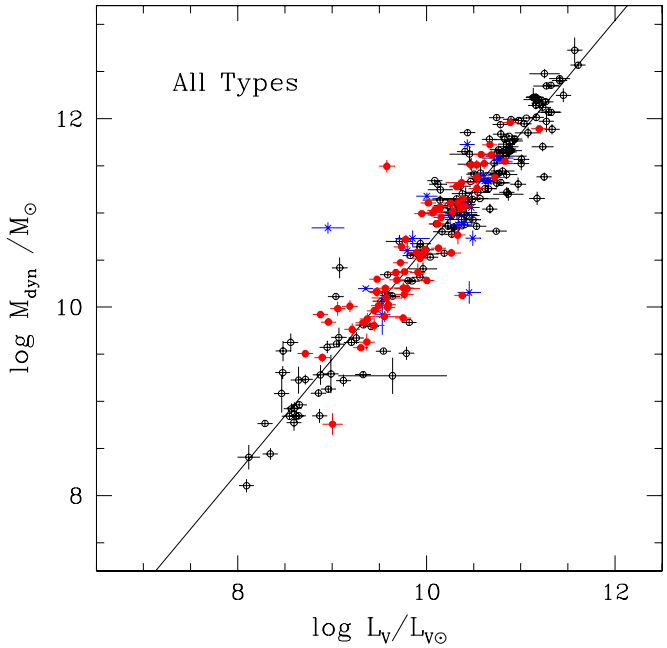

Figure 3. $M_{\rm dyn}$ vs. total visual luminosity L_V for all galaxies in the GCS catalog. The E/dE systems are plotted as open circles, S0 as red filled symbols, and S/Irr systems as blue crosses. An arbitrary offset of +0.2 dex has been applied to $(\log M_{\rm dyn})$ for the S0 points, and +0.3 dex to the S/Irr points to bring them in line with the E-galaxy solution (see text). The diagonal line shows the best-fit linear solution to the ellipticals as in the previous figure.

(A color version of this figure is available in the online journal.)

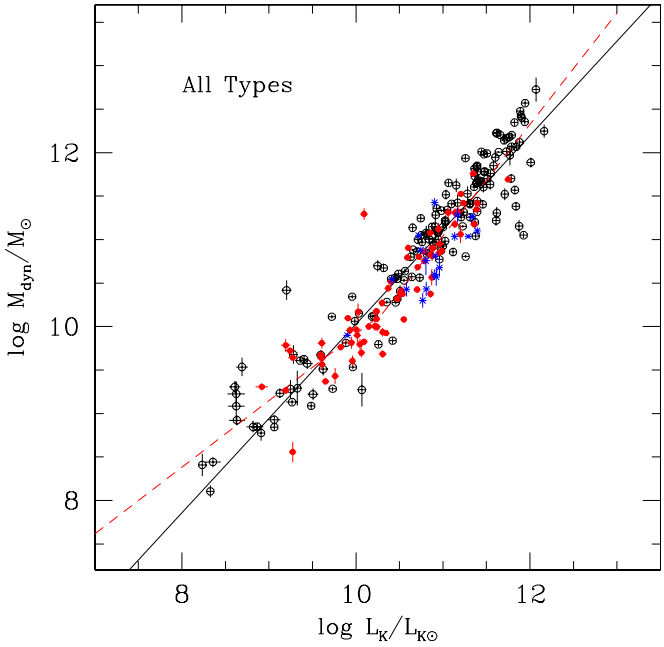

Figure 4. $M_{\rm dyn}$ plotted vs. total K-band luminosity L_K for the galaxies in the GCS catalog. The E/dE systems are plotted as open circles, S0 as red filled symbols, and S/Irr systems as blue crosses. The solid diagonal line shows the best-fit linear solution to the entire sample, as described in the text, whereas the dashed line shows the two-part solution over the bright and faint ranges as in Table 2.

(A color version of this figure is available in the online journal.)

has a very similar scatter of ± 0.26 dex. However, unlike L_V (Figure 3), the relation exhibits a noticeable nonlinearity where the brighter galaxies follow a steeper slope. Splitting the data at $M_K = -22.4$ (or $\log L_K/L_{K\odot} = 10.3$) gives the two additional solutions listed in Table 2, where $M_{\rm dyn} \sim L_K^{0.765\pm0.060}$ for fainter galaxies and $M_{\rm dyn} \sim L_K^{1.260\pm0.048}$ for brighter ones.

In summary, both V and K luminosities in our catalog can act as similarly precise indicators of galaxy dynamical mass. Where necessary, in the discussion below we choose to use L_V because it is available for the entire catalog of galaxies.

3.1. Cluster Population and Galaxy Scale Parameters

We next plot total cluster population $N_{\rm GC}$ versus the other listed scaling parameters: L_V, σ_e, R_e, and $M_{\rm dyn}$. These are displayed in Figures 5–9, and selected best-fit solutions are listed in Table 2. Comparison with the remaining quantity in the list, the SMBH mass, is a special topic that has been the subject of discussion in several recent papers, including Spitler & Forbes (2009, hereafter S09), Burkert & Tremaine (2010), Harris & Harris (2011), Snyder et al. (2011), Sadoun & Colin (2012), Rhode (2012), and Harris et al. (2013), and will not be repeated here.

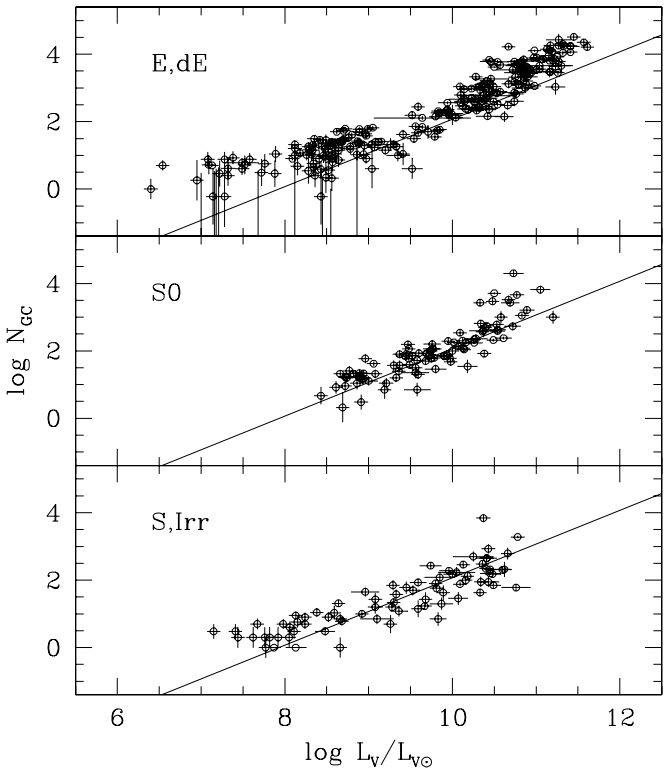

Figure 5. Top panel: total number of globular clusters N_{GC} plotted vs. the visual luminosity of the host galaxy, for elliptical galaxies. Middle panel: the same plot for S0 galaxies. Bottom panel: the same plot for spiral and irregular galaxies. In all three panels, the sloped line denotes a specific frequency $S_N \equiv 1$.

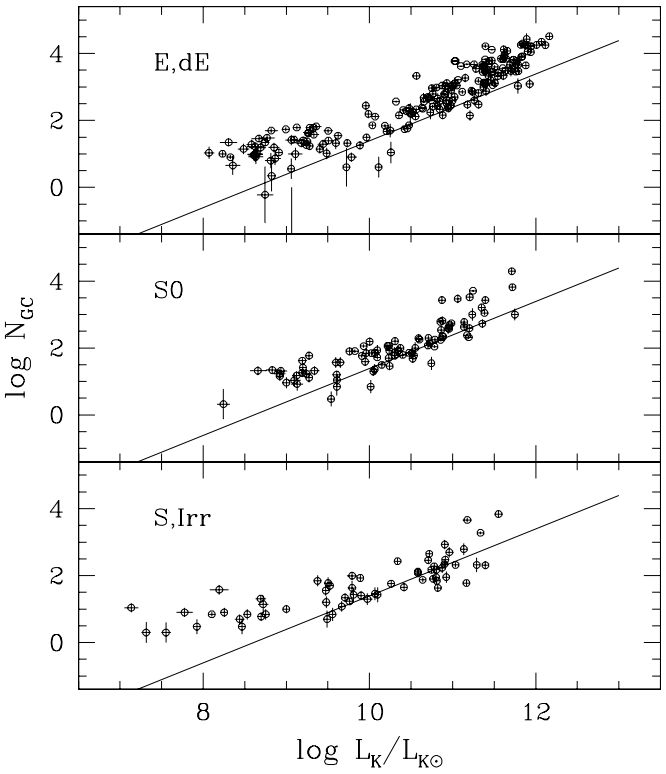

Figure 6. Top panel: total number of globular clusters N_{GC} plotted vs. the K-band luminosity of the host galaxy, for elliptical galaxies. Middle panel: the same plot for S0 galaxies. Bottom panel: the same plot for spiral and irregular galaxies. In all three panels, the sloped line denotes a specific frequency $S_N \equiv 1$.

The most easily observable relation is between N_{GC} and the galaxy V luminosity, which was also historically the first to be discussed in the literature (Jaschek 1957; Hanes 1977; Harris & Racine 1979; Harris & van den Bergh 1981). The data for all the systems in the current catalog are shown in Figure 5. As has been found in all earlier discussions, N_{GC} increases very roughly in direct proportion to host galaxy luminosity, but obvious systematic deviations occur at both the high- and low-luminosity ends of the scale, and between E/S0 systems and S/Irr ones.

In Figure 6, we show the correlations between N_{GC} and near-IR luminosity M_K. The pattern is very much the same, and the scatter quite similar to the previous figure. Since the N_{GC}–M_K graph appears to give much the same information, and M_V^T is available for a larger sample of galaxies, we stick primarily with the use of the visual-luminosity data in the following discussion.

The connection between galaxy size and GC population is most often presented in terms of the specific frequency (Harris & van den Bergh 1981),

$$S_N \equiv N_{GC} \times 10^{0.4(M_V^T+15)} = (8.51 \times 10^7)\,\frac{N_{GC}}{L_V/L_{V\odot}}. \quad (4)$$

In the K band, if we adopt a typical color index $(V-K) \simeq 3.2$ for E galaxies and bulges (e.g., Michard 2005), then the equivalent relation is

$$S_N \equiv N_{GC} \times 10^{0.4(M_V^T+18.2)} = (4.1 \times 10^8)\,\frac{N_{GC}}{L_K/L_{K\odot}}. \quad (5)$$

The trend of S_N versus M_V^T is shown in Figure 10, for the three subsets of data combined. The characteristic U-shaped distribution is the most prominent feature of the diagram: the intermediate-luminosity galaxies form a rather tight grouping in a "valley" around $S_N \simeq 1$, and the dwarfs and supergiants at opposite ends show much larger scatter and higher mean S_N. This distribution was apparent even in the first discussion

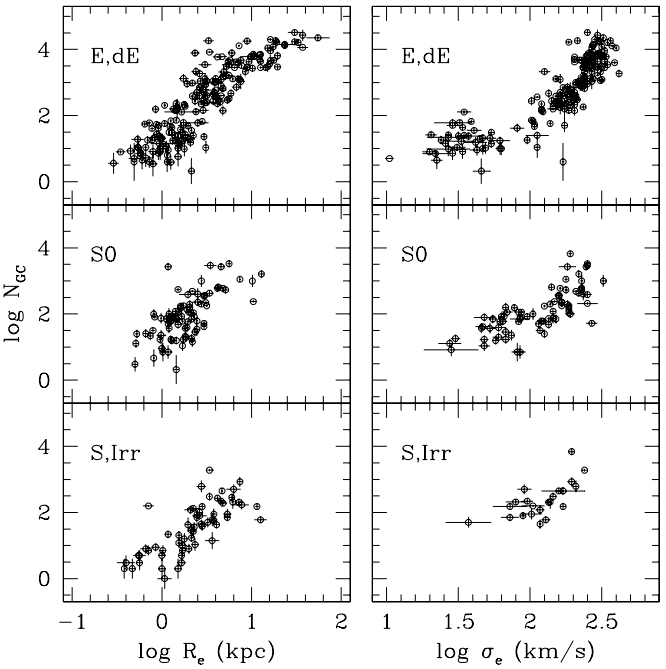

Figure 7. Left panels: total number of globular clusters N_{GC} plotted vs. the effective radius R_e of the host galaxy. Elliptical, S0, and S/Irr galaxy types are plotted separately. Right panels: total number of globular clusters N_{GC} plotted vs. the bulge velocity dispersion of the host galaxy.

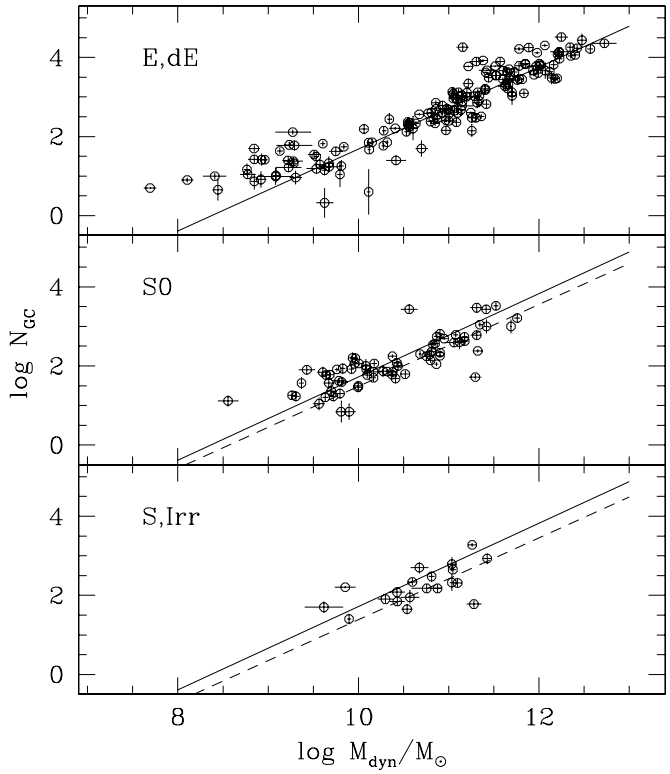

Figure 8. Correlation of GC population size N_{GC} vs. the dynamical mass $M_{dyn} = 4R_e\sigma_e^2/G$. The data are shown separately for ellipticals, S0s, and spirals as in previous figures. In each panel the solid diagonal line shows the best-fit solution for the luminous E galaxies as discussed in the text, i.e., excluding the dwarfs. In the middle panel, the dashed line is the E-galaxy solution shifted downward by 0.2 dex, while in the lower panel the dashed line is the E line shifted downward by 0.3 dex (see text).

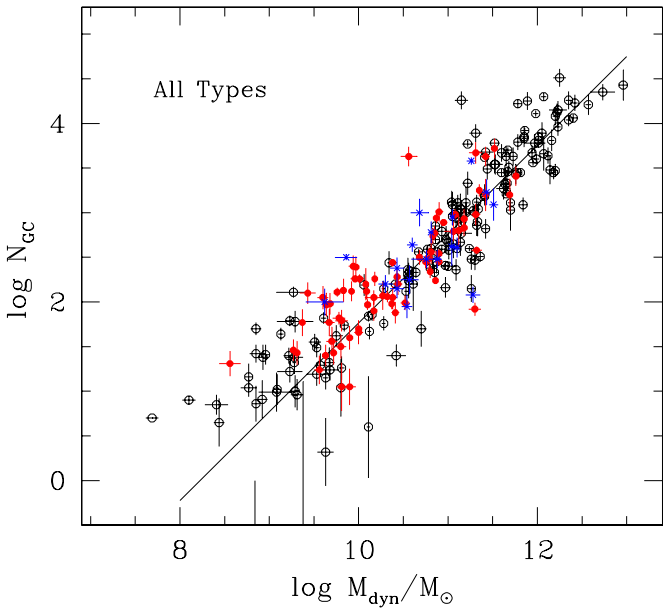

Figure 9. Correlation of GC population size N_{GC} vs. the dynamical mass $M_{dyn} = 4R_e \cdot \sigma_e^2/G$. E galaxies are plotted as open circles, S0s as solid red circles, and spirals as blue crosses. The N-values for the S0 and spiral types have been normalized to the E-galaxy level as described in the text. The solid diagonal line shows the best-fit solution for all galaxies with $M_{dyn} > 10^{10}\,M_\odot$. (A color version of this figure is available in the online journal.)

of specific frequency from a sample more than an order of magnitude smaller (see Figure 4 of Harris & van den Bergh 1981). Two notable recent versions with extensive discussions are given by P08 and Georgiev et al. (2010, hereafter G10), which build on the newer surveys and particularly fill in the lower-luminosity range more extensively than before.

In general the highest specific frequencies are found either in some E supergiants (particularly the cD or BCG giants) or in dwarf spheroidals and nucleated dE,N galaxies.[3] S0 and disk galaxies have systematically lower S_N than ellipticals, field Es have lower S_N than ones in rich clusters of galaxies, and dEs in denser environments favor higher S_N (e.g., Hanes 1977; Harris & van den Bergh 1981; van den Bergh 1982, 2000; Durrell et al. 1996; Harris 2001; Brodie & Strader 2006; and P08).

In most galaxies there are two clearly identifiable subsets of GCs that separate out by color or metallicity: the blue (metal-poor) population and the red (metal-rich) ones (e.g., Peng et al. 2006; Harris 2009; Mieske et al. 2010). The ratio N(red)/N(blue) is dependent on galaxy size, with GC populations in lower-luminosity galaxies of all types progressively more dominated by the metal-poor component (Peng et al. 2006). The blue GCs are likely to be the remnants of the very earliest star-forming stages of hierarchical merging, emerging out of the gas-rich and metal-poor protogalactic dwarfs (e.g., Burgarella et al. 2001; Moore et al. 2006; and P08), or added later by accretion of low-mass metal-poor satellites. With photometric data of sufficient quality, it is also possible to define S_N or the GC mass fraction for red and blue types separately (e.g., Rhode et al. 2005, 2007; Brodie & Strader 2006; Spitler et al. 2008; Forte et al. 2009). However, many of the galaxies in our catalog do not have sufficient photometric data to evaluate the blue/red ratios accurately, and we do not pursue this question here. New photometric data aimed at obtaining high-quality blue/red population ratios for more galaxies would be of great interest. In particular, it would be important to know how much of the scatter around the mean S_N relation at a given galaxy luminosity might be due solely to differences in the relative number of blue GCs (and thus the efficiency of cluster formation at the earliest stages). The references cited above should be seen for more complete discussion.

3.2. Other Correlations for N_{GC}

Going beyond specific frequency, we have explored more general correlations of N_{GC} versus combinations of scale size and velocity dispersion. We might, for example, hope to find choices which would more nearly linearize the trend of N_{GC} over the *entire* galaxy luminosity range from dwarfs to supergiants.

Neither R_e nor σ_e by itself is a good predictor of GC population. As seen in Figure 7, N_{GC} versus those quantities exhibits quite a lot of scatter and behaves nonlinearly. The exception here is $N(R_e)$ for the spiral and irregular galaxies, which yields a roughly useful scaling in the cases where σ_e is not available (see discussion below).

N_{GC} versus M_{dyn} is plotted in Figure 8 for the three galaxy types, and in Figure 9 for all galaxies combined. Similar trends of GCS numbers versus mass are also discussed by P08, S09, and G10. The significant difference compared with our work is that these previous studies employed *photometrically* determined masses (e.g., the combination of a near-IR luminosity and

[3] At the top end, the anomalously high-S_N values seen in Figure 10 for four S0 or S galaxies are those for NGC 6041A, UGC 3274, A2152-2, and IC 3651. All are distant and luminous systems in rich clusters of galaxies, and close inspection of images suggests that they may simply be misclassified E/cD systems.

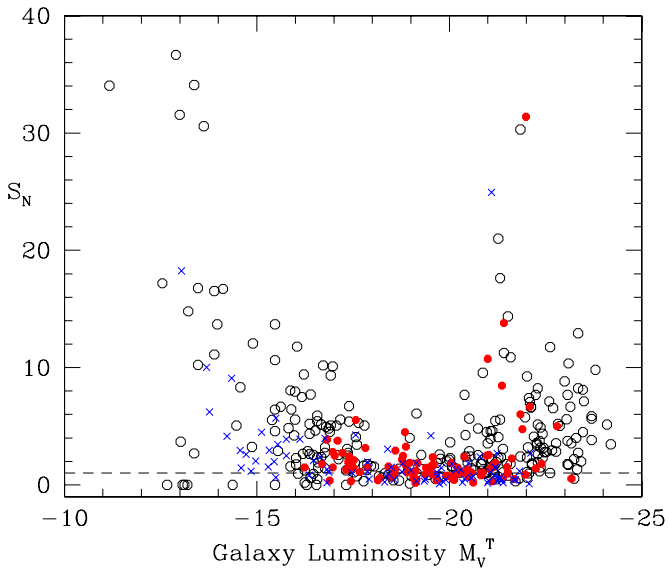

Figure 10. Specific frequency S_N vs. the absolute visual magnitude M_V^T of the host galaxy. E and dE galaxies are plotted as open circles, S0 systems as solid red circles, and spirals or irregulars as blue crosses. The horizontal line at bottom shows $S_N = 1$.

(A color version of this figure is available in the online journal.)

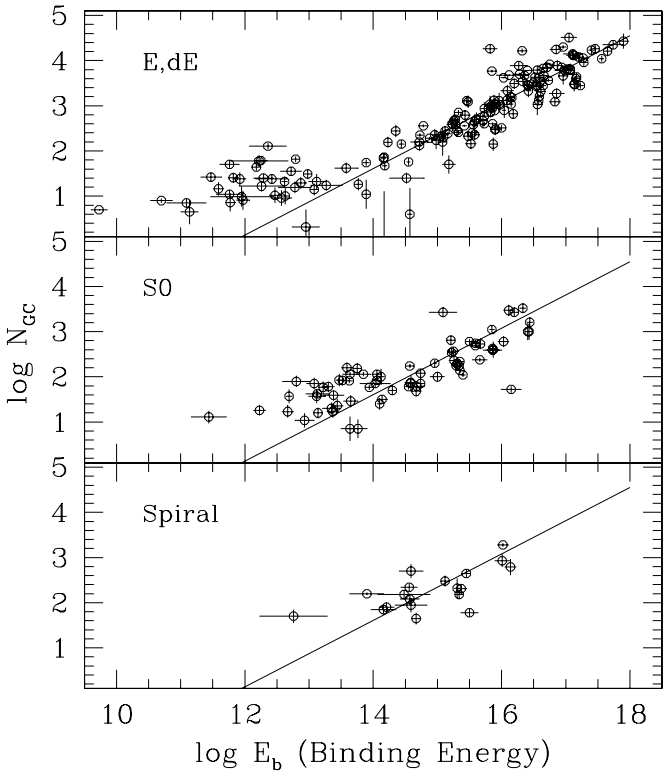

Figure 11. Correlation of GC population size N_{GC} vs. the binding energy $E_b \sim R_e \cdot \sigma_e^4$, as described in the text. In each panel the solid diagonal line shows the best-fit solution for the luminous E galaxies, i.e., excluding the dwarfs.

an assumed mass-to-light ratio), whereas we use M_{dyn}, which stands independently of photometric indicators.

For galaxy masses $>10^{10}\,M_\odot$, we find that $N_{GC} \sim M_{dyn}^{1.04\pm0.03}$. That is, GCS population increases in almost exactly direct proportion to galaxy mass. For the smaller galaxies, the scaling is much shallower at $N_{GC} \sim M_{dyn}^{0.4}$ and these also exhibit larger scatter (see particularly Figure 9). We find as well that the S0-type galaxies lie below the ellipticals by Δ log $N_{GC} \simeq -0.2$ dex, while the spiral types fall even further below the ellipticals by -0.3 dex (again, no irregulars appear in this plot). In short, *if* the same definition of M_{dyn} is valid for disk galaxies and ellipticals (cf. the caveats mentioned earlier), then disk galaxies have fewer clusters per unit bulge mass than do ellipticals, by factors of 1.5–2. This point is discussed more extensively by G10. To plot up Figure 9 we have applied these offsets to the S and S0 types to bring them back to the E/dE line.

In Figure 6, we show N_{GC} now plotted against K-band infrared luminosity. In principle, if near-IR luminosity is a valid proxy for total stellar mass, then this graph should reveal the same basic trend as does Figure 9. It does show the same trend, but the scatter is similar to the correlations with L_V and so is not additionally useful for the present purposes.

In addition to $M_{dyn} \sim R_e\sigma_e^2$, another quantity used occasionally in the literature, especially for pressure-supported systems such as star clusters, molecular clouds, or E galaxies, is the system's binding energy $E_b \sim M\sigma^2 \sim R_e\sigma_e^4$ (e.g., McLaughlin 2000; Hopkins et al. 2007; Snyder et al. 2011). For completeness we show the correlation of N_{GC} and E_b in Figure 11, where numerically we define $E_b = M_{dyn}(\sigma_e/[200\,\mathrm{km\,s^{-1}}])^2$. Once again, the luminous galaxies (log $E_b > 13.5$) form a well-defined relation close to $N_{GC} \sim E_b^{3/4}$, with total scatter quite similar to the previous solution between N_{GC} and M_{dyn} (see Table 2). However, the dwarf galaxies stand even further off the mean line than before, so there appears to be no additional advantage to using E_b as a predictor of GC population.

Going in the opposite direction to a smaller power of σ_e has the numerical effect of reducing its importance and bringing the dwarfs closer to the giant-galaxy line. We have explored a range of different empirical combinations and, as an example, we show the case for (log N_{GC}) against the direct product (log $R_e\sigma_e$) in Figure 12. This result comes close to giving a nearly linear correlation with encouragingly low scatter, over the *entire luminosity range* of galaxies from the smallest dwarfs to the largest supergiants, a range of five orders of magnitude in mass. In performing the fit we have deleted the five most deviant points (three dwarfs, two giants), leaving $N = 158$ galaxies to determine the solution. In Figure 12 the E-galaxy solution is also shown superimposed on the data for the 72 S0 and 19 spiral systems. Again, the E solution adequately matches the S0s for a -0.2 dex shift in log N_{GC}, and matches the spirals for a -0.3 dex shift (shown as the dashed lines in the lower two panels).

In brief, we find that *the total GC population of a galaxy is accurately predicted by the simple product of the galaxy's effective radius R_e and bulge velocity dispersion σ_e*. The specific relation for the E galaxies is

$$N_{GC} = (600 \pm 35)\left[\left(\frac{R_e}{10\,\mathrm{kpc}}\right)\left(\frac{\sigma_e}{100\,\mathrm{km\,s^{-1}}}\right)\right]^{1.29\pm0.03}. \quad (6)$$

The same relation can also be used for S0 and spiral types, with the zero-point shifts given above.

This simple relation is not useful for late-type spiral or irregular galaxies where σ_e is not defined or not measurable. In those cases, a rough but still useful predictor of N_{GC} appears to be the effective radius R_e alone, as seen in Figure 7 (lower left panel). For these types of galaxies, we find

$$N_{GC} = (38 \pm 7)(R_e/2.5\,\mathrm{kpc}) \quad (7)$$

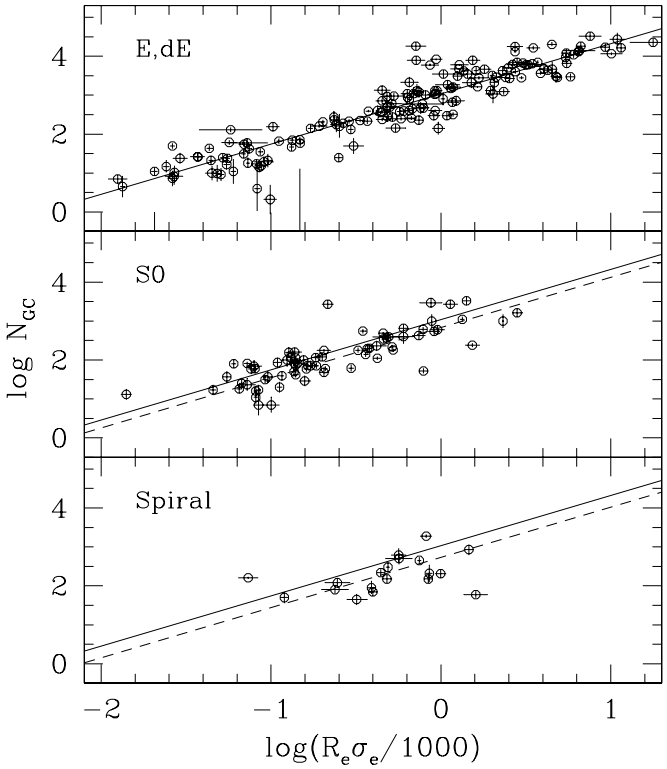

Figure 12. GC population size N_{GC} vs. $(R_e\sigma_e)$ as defined in the text. The data are shown separately for ellipticals, S0s, and spirals as in previous figures. In each panel the solid diagonal line shows the best-fit solution for the E galaxies, but now including both dwarfs and giants. In the second panel, the dashed line shows the E-galaxy line shifted downward by 0.2 dex, while in the lower panel the dashed line shows the E-galaxy solution shifted down by 0.3 dex.

(listed in its log/log form in Table 2). The scatter in this case is ±0.53 dex in log N_{GC}, significantly higher than for the other relations presented above, and reflecting the intrinsically wide range of GC systems found in star-forming dwarf galaxies. Nevertheless, it should be useful for giving first-order estimates if no other recourse is available.

3.3. Specific Mass and Galaxy Scale Parameters

The total number of GCs in a galaxy is only a proxy for a more physically relevant quantity, the total stellar *mass* M_{GCS} contained in all the GCs. Ultimately, we would like to know the typical fraction of baryonic mass or total halo mass taken up by the GCs. Here we use the "specific mass" defined as a percentage of the previously calculated dynamical mass of the host galaxy,

$$S_M = 100\frac{M_{GCS}}{M_{dyn}}. \quad (8)$$

This ratio should in principle be similar to the definition $S_M = 100M_{GCS}/M_{G\star}$ used by P08, since as discussed above, M_{dyn} is nearly equal to the total bulge stellar mass with minor contributions from either dark matter or gas (except for major star-forming systems). By comparison, G10 use $S_M = 100M_{GCS}/(M_\star + M_{gas})$, which can be significantly different for either gas-rich dwarfs or cD-type systems with massive amounts of hot halo gas. Perhaps more importantly, however, our discussion of S_M differs from those of P08, S09, or G10 in that they used *photometrically estimated* stellar masses $M_\star$ versus our dynamical masses.

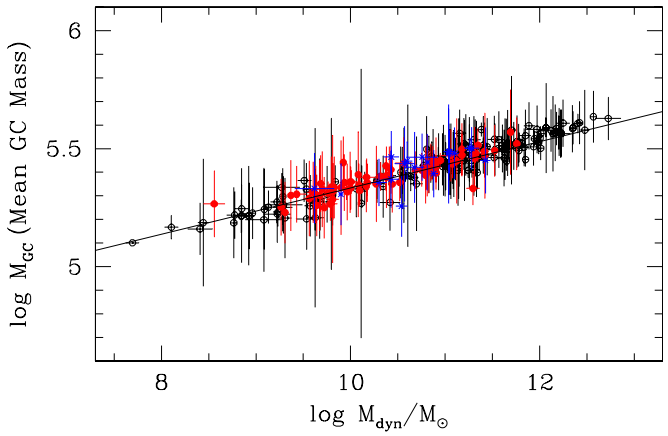

Figure 13. Mean globular cluster mass $\langle M_{GC}\rangle$ vs. galaxy mass M_{dyn}. Here, the mean GC mass is defined as $\langle M_{GC}\rangle = M_{GCS}/N_{GC}$ and the total mass in the globular cluster system is calculated as described in Section 3.3. Symbols for the three galaxy types (E, S0, S/Irr) are as in previous figures. The diagonal line gives the best-fit relation $\langle M_{GC}\rangle \sim M_{dyn}^{0.098}$ (Table 2).
(A color version of this figure is available in the online journal.)

To define S_M we need to add up the masses of the GCs in a given galaxy, or equivalently find the mean GC mass. For studies of GCSs such as the Virgo Cluster survey (Peng et al.) or ones in very nearby galaxies, it is possible to obtain a nearly complete census of all the clusters in a given galaxy and explicitly add them up one by one. For most of the galaxies in our catalog, however, we must adopt a more broad-brush procedure in hopes of identifying first-order trends. What helps considerably is the empirical fact that the GCLF has a consistent, predictable shape across all galaxies, which conveniently allows us to scale N_{GC} to M_{GCS} fairly straightforwardly.

Usually the GCLF is represented by a simple Gaussian in number of GCs per unit magnitude interval, $n(M_V)$, with a characteristic peak μ_V and standard deviation σ_V. More detailed analysis suggests that a slightly asymmetric form such as the "evolved Schechter function" developed by Jordán et al. (2006, 2007) is a better match to the data. However, this is only a minor concern because the total mass in the GCS is dominated by the clusters brighter than the peak (turnover) point of the GCLF; the clusters fainter than the turnover make up typically only ≃20% of the total GCS mass. Thus, the normal Gaussian-type analytical approximation where σ_V is determined by the bright half of the GCLF remains quite useful.

A more important consideration is that μ_V and σ_V depend on galaxy luminosity, in the sense that the GCLF becomes broader and brighter for bigger galaxies. To integrate over the GCLF, we follow the relations derived by Jordán et al. (2006) and V10, adopting $\mu_V = -7.4 + 0.04(M_V^T + 21.3)$ and $\sigma_V = 1.2 - 0.10(M_V^T + 21.3)$, where the zero points are normalized to the Milky Way.[4] Finally, to convert GC luminosity to mass, we use a constant $(M/L)_V = 2$ (McLaughlin & van der Marel 2005).[5] Figure 13 shows the resulting trend of mean individual GC mass versus galaxy mass M_{dyn} (where now $\langle M_{GC}\rangle \equiv M_{GCS}/N_{GC}$). The residual scatter around this relation is simply the visible result of the galaxy-to-galaxy differences in the calculated $M_{dyn} = f(R_e, \sigma_e)$ for a given

[4] The exception is that we set a lower bound $\sigma_V(\min) = 0.5$. Inspection of the data from V10 shows that the deduced slope $\Delta\sigma/\Delta m = -0.10$ depends heavily on the more luminous galaxies, whereas for the dwarfs there is mainly a large scatter with no clear trend.

[5] We note that S09 use a constant μ_V and σ_V to calculate M_{GCS}.

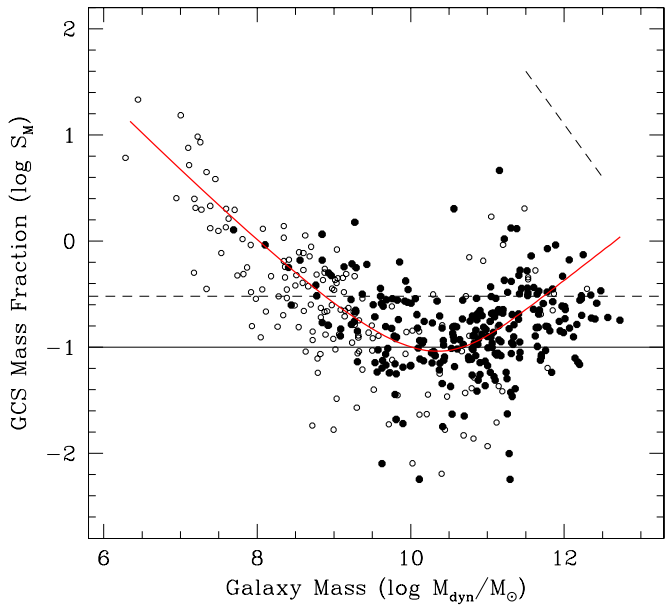

Figure 14. Specific mass $S_M = 100(M_{GCS}/M_{dyn})$ vs. host galaxy mass. Solid dots are dynamical masses M_{dyn} calculated from (R_e, σ_e), while open circles are masses estimated from L_V and Equation (3), for galaxies without measurements of R_e and σ_e. The solid diagonal line at upper right shows the effect of changing M_{dyn} by 1.0 dex (an increase in M_{dyn} yields a proportionate decrease in $S_M \sim M_{GCS}/M_{dyn}$). The horizontal line at $S_M = 0.1$ is the approximate average level reached for the intermediate-luminosity galaxies where star formation is maximally efficient. Eighty percent of all galaxies fall below the dashed horizontal line at $S_M = 0.3$ (see text). The superimposed curve is the interpolation model fit discussed in Section 4.2.

(A color version of this figure is available in the online journal.)

galaxy luminosity. This graph would be a dispersionless relation if, as in other papers, we had used galaxy *luminosity* to determine galaxy mass. The overall trend is listed in Table 2 and shown in Figure 13 and is well matched by a single power law, $\langle M_{GC} \rangle = (2.26 \times 10^4) M_{dyn}^{0.098}$ in solar masses.

The correlation solution for GCS mass versus galaxy mass, for the E galaxies with $L > 10^{10}\, L_\odot$ (Table 2), yields $M_{GCS} \sim M_{dyn}^{1.16\pm0.04}$, slightly but significantly steeper than the $N_{GC} \sim M_{dyn}^{1.04}$ dependence found earlier. The difference is a direct result of the second-order trend for mean GC mass to increase with host galaxy size. For the smaller E galaxies, the mean trend is $M_{GCS} \sim M_{dyn}^{0.46\pm0.10}$, again quite similar to the dependence of N_{GC} on M_{dyn}.

The plot of S_M versus M_{dyn} is shown in log/log form in Figure 14. The overall distribution is roughly similar to that for S_N (Figure 10), though with less scatter at either the high-luminosity or low-luminosity ends. This reduced scatter is partly a result of our use of dynamical masses rather than photometric masses for the galaxies (for example, two giant ellipticals may have the same luminosities, but if one of them is a cD-type or BCG, it will usually have a larger effective radius or central velocity dispersion and thus a higher dynamical mass).

The practical penalty for using S_M instead of S_N is that we cannot strictly include as many datapoints because we need to have both R_e and σ_e to determine M_{dyn}. We therefore supplement the dynamical data by adding in photometrically calculated masses from the known conversion between L_V and M_{dyn}, from Equation (3) and Table 2. These secondary masses are added for the galaxies without measured R_e and σ_e. As is evident in Figure 14, the extra points are particularly valuable for the lower-luminosity galaxies.

4. DISCUSSION

4.1. Population Scaling Relations

We can gain some more understanding of why the relation shown in Figure 12 between cluster population and $(R_e\sigma_e)$ works by looking further at the scaling relations among galaxy mass, luminosity, size, and velocity dispersion. For the giant ellipticals ($L > 10^{10}\, L_\odot$), direct fits of each of R_e and σ_e versus luminosity give $R_e \sim L^{0.66\pm0.033}$ and $\sigma_e \sim L^{0.285\pm0.017}$. Combining these then predicts $(R_e\sigma_e) \sim L^{0.95\pm0.04} \sim M_{dyn}^{0.79\pm0.04} \sim N_{GC}^{0.76\pm0.04}$, using the other correlations in Table 2 to translate from L to M_{dyn} and then to N_{GC}. Inverting the result then gives $N_{GC} \sim (R_e\sigma_e)^{1.31\pm0.07}$, which closely matches what we obtain from the direct solution in Figure 12 and Table 2.

The dwarf galaxies obey somewhat different scalings among size, dispersion, and luminosity, namely, $R_e \sim L^{0.26\pm0.06}$ and $\sigma_e \sim L^{0.32\pm0.06}$. Combining these leads to $(R_e\sigma_e) \sim M_{dyn}^{0.48\pm0.07}$. However, this shallower trend is partly compensated by the shallower dependence of cluster population on mass for the dwarfs (Table 2), $N_{GC} \sim M^{0.37\pm0.09} \sim (R_e\sigma_e)^{0.78\pm0.17}$. The luminosity range of the dwarf Es is small enough that they can accommodate a relatively wide range of slopes, permitting a single linear relation across the entire range from dwarf spheroidals to supergiants to be a workable representation. Said differently, the GC population of a galaxy can be seen as another outcome of the FP for early-type galaxies.[6]

4.2. Mass Fractions and Formation Efficiency Parameters

Discussion of the specific frequency and specific mass S_N and S_M quickly leads to the question of GC formation efficiency—the original reason for defining these ratios. A summary of the thinking during the early (pre-ΛCDM) literature can be found in Harris (2001). A more recent view with growing evidence is that the GCs, which are compact stellar subsystems emerging from the densest and most massive sites of star formation, could be the objects that form earliest in any starburst, followed by the bulk of the field stars and the lower-mass star clusters that soon dissolve into the field. First ideas along these lines were explored by Blakeslee (1997), McLaughlin (1999), Kavelaars (1999), and Harris & Harris (2002), pointing to the possibility of a universal GC formation efficiency *per unit baryonic mass* including both stars and gas. If the later rounds of star formation *after* GC formation are truncated or severely reduced by any combination of external or internal quenching, then the resulting S_N or S_M observed long after the fact is a marker of how well the quenching worked. High-S_N systems thus would be *field-star deficient* (not "cluster-rich") because the star formation was prevented from running to completion. This interpretation has been developed further by P08, G10, and Spitler (2010); in particular, P08 estimate quantitatively that in dwarf galaxies the peak star formation epoch lagged the peak GC formation epoch by 350–600 Myr.

Different mechanisms for shutting down star formation will operate at the opposite extremes of the galaxy mass range. For the dwarfs with their small potential wells, internally driven feedback including starburst winds, photoionization, and ultimately supernovae (SNe) may eject a large fraction of the

[6] If we assume more generally that $N_{GC} \sim R_e^a \sigma_e^b$, it can be shown from the scalings between R_e, σ_e, and L listed above that any pair of exponents where $a \simeq 6.9b$ will work for both the giants and dwarfs. However, the combination $N \sim (R\sigma)^{1.3}$ has the strong advantage of simplicity and reproduces the actual data well.

gas, while external quenching from tidal stripping of gas or external UV fields can also reduce the star formation efficiency (SFE). For the most massive galaxies, active galactic nucleus (AGN) feedback and virial shock heating of infalling gas will lower the SFE (Dekel & Silk 1986; Dekel & Woo 2003; Dekel & Birnboim 2006; Bower et al. 2006).

The maximum SFE should then happen for intermediate-mass galaxies which are massive enough to hold their star-forming gas against SN and starburst winds, but in which AGN feedback and shock heating are not intense enough to have much effect. Much recent literature has addressed this issue by tracing the change in the ratio $M(\mathrm{halo})/M(\mathrm{baryon})$ versus galaxy size, which displays the same U-shaped distribution that we see in the S_N and S_M curves. To mention only two recent studies, Shankar et al. (2006) identify SFE (max) at a stellar mass $M_\star \simeq 6.3 \times 10^{10}\ M_\odot$ or $M(\mathrm{halo}) \simeq 10^{12}\ M_\odot$, while from a combination of direct stellar mass and halo mass observational determinations Leauthaud et al. (2012) find the SFE maximum to be at $M_\star \simeq 4 \times 10^{10}\ M_\odot$.

Viewed in this light, the *minimum* of the S_M or S_N distributions becomes perhaps the most interesting region of those diagrams. The baseline ratios $S_N \simeq 1$ and $S_M \simeq 0.1$ essentially tell us, *in the galaxies where star formation was globally the most efficient*, what mass fraction went into the dense compact systems that we *now* see surviving as GCs. That is, *these baseline values reveal what the "natural" GC formation efficiency is when any disruption or quenching of star formation is at its least important.*

This present-day mass fraction is, however, only a lower limit to the value at the time of formation, because (1) many low-mass or low-density star clusters are disrupted or dissolved over the subsequent Hubble time, and (2) even the surviving ones that started as the densest, most massive clumps have lost a large fraction of their initial mass through a combination of early rapid mass loss (expulsion of residual gas, and SNe and stellar winds from massive stars) and later dynamical erosion. The current literature (Trenti et al. 2007; McLaughlin & Fall 2008; Vesperini 2010) indicates that the individual GCs that have survived to the present should have been ~10 times more massive when they were protoclusters than they are now. The conclusion we draw from these arguments is that the surviving GCs represented at least 1% of the star formation mass fraction in the maximally efficient intermediate-mass galaxies. In either dwarf or supergiant galaxies, however, where S_M may be an order of magnitude higher, the GCs we see today could—as protoclusters—have taken as much as 10% of the gas that successfully formed stars. And these mass fractions must only be lower limits to the amounts of star-forming gas that went into young star clusters, after accounting for the clusters that did not survive to the present.

The interpretation that M_{GCS} is driven by the amount of gas mass initially present in the galaxy's potential well (and not the gas mass that was actually consumed in star formation) then raises the possibility that M_{GCS} should be more nearly proportional to M_{halo}, or the total depth of the galaxy potential well. This direction has been explored by Blakeslee (1997), McLaughlin (1999), Spitler et al. (2008), P08, S09, and G10. Following the notation of G10, we denote $\eta \equiv M_{\mathrm{GCS}}/M_{\mathrm{halo}}$. For the dwarf galaxies in particular (discussed at greater length by P08 and G10), our derivation that $M_{\mathrm{GCS}} \sim M_{\mathrm{dyn}}^{0.46\pm0.10}$ is in excellent agreement with the scaling $M_{\mathrm{halo}} \sim M_\star^{0.46}$ obtained by Leauthaud et al. (2012) if we assume that $M_{\mathrm{GCS}} \propto M_{\mathrm{halo}}$ and also $M_\star \simeq M_{\mathrm{dyn}}$ as above.

To derive the "absolute" GC formation efficiency parameter η from our new sample of galaxies, we need to adopt a stellar-to-halo mass conversion relation $M_{\mathrm{halo}} = f(M_\star)$, or else its inverse. By hypothesis we also simply use $M_\star \simeq M_{\mathrm{dyn}}$ and $\eta = const$ as mentioned above. These steps then directly link M_{halo} to M_{GCS} and $M_\star$, and the assumed value of η can be varied until a match is achieved with our data. Our specific approach is to fix η by requiring the resulting S_M versus $M_\star$ curve to pass through the baseline $S_M \simeq 0.1$ for the intermediate-mass galaxies.

One such conversion between $M_\star$ and M_{halo} is given by Behroozi et al. (2010) and Leauthaud et al. (2012), derived from a combination of methods for measuring M_{halo} and $M_\star$ over a wide range of luminosity regimes (see Equation (24) from Behroozi or Equation (13) from Leauthaud). Their empirical model shows a clear rise in the ratio $M_{\mathrm{halo}}/M_\star$ at the low-mass and high-mass ends with a minimum at intermediate galaxies. However, their model function and parameters give a curve for S_M that is too steep at each end to be satisfactory in detail for our purposes. A flexible and simpler conversion relation from Yang et al. (2008) and also used by S09 is

$$M_\star = M_0 \frac{(M_{\mathrm{halo}}/M_1)^{\alpha+\beta}}{(1 + M_{\mathrm{halo}}/M_1)^{\beta}}. \quad (9)$$

To use this, we assume a value for M_{halo}, which determines $M_\star$ (which by hypothesis equals our M_{dyn}). Finally $S_M = 100 \cdot M_{\mathrm{GCS}}/M_\star$, which then defines a point on Figure 14. Repeating for a wide range of M_{halo} then defines a complete S_M versus M_{dyn} curve.

An illustrative fit of this model to the GCS data is shown as the solid curve in Figure 14. This curve uses the parameters $\eta = 6.0 \times 10^{-5}$, $\log M_0 = 9.98$, and $\log M_1 = 10.7$ along with exponents $\alpha = 0.64$, $\beta = 2.88$.[7] At either the low-mass or high-mass end of the scale, the S_M curve asymptotically approaches a simple power law. At the high-mass end, where (M_{halo}/M_1) becomes large, it can quickly be shown that $S_M \rightarrow \mathrm{const} \cdot M_{\mathrm{dyn}}^{(1-\alpha)/\alpha}$, which for our fitted value $\alpha \simeq 0.64$ gives $S_M \sim M_{\mathrm{dyn}}^{0.563}$. At the low-mass end where (M_{halo}/M_1) is small, then $S_M \rightarrow \mathrm{const} \cdot M_{\mathrm{dyn}}^{-1+1/(\alpha+\beta)}$, which for $\beta = 2.88$ gives $S_M \sim M_{\mathrm{dyn}}^{-0.716}$.

Our estimated $\eta \simeq 6 \times 10^{-5}$ represents the absolute efficiency of GC formation. By comparison, through different combinations of methods for deriving the various masses and luminosities, G10 find a mean $\langle\eta\rangle \simeq 6 \times 10^{-5}$, while S09 find $\eta \simeq 7 \times 10^{-5}$. The agreement among these discussions is well within the scatter we can expect given the different assumptions for the definition of S_M and the methods for finding galaxy luminosities, stellar masses, and dark-halo masses.

We have suggested in the discussion above that the galaxy mass where S_M reaches a minimum represents the level where SFE was the highest. The S_M interpolation curve in Figure 14 reaches a minimum at $M_{\mathrm{gal}} \simeq 2.5 \times 10^{10}\ M_\odot$. Within the accuracy permitted by the scatter around the curve, this minimum point is strikingly similar to the galaxy-based estimates of $M_{\mathrm{gal}} \sim 5 \times 10^{10}\ M_\odot$ mentioned above for the point of maximum SFE, and emerges from quite a different line of argument. Yet another piece of information in line with these results is recent evidence (Spolaor et al. 2009, 2010; Tortora et al. 2010) that the maximum *metallicity gradient* within galaxies occurs near

[7] The power-law-like slopes of the model curve at the high- and low-mass ends are quite sensitive to the choices of (α, β), and the values we find to give a good fit are slightly different from the ones used by S09. Again, they used a different, simpler prescription for $\langle M_{\mathrm{GC}}\rangle$ and thus M_{GCS}; a smaller GCS data set; and a different prescription for computing galaxy masses.

$M_{\rm gal} \sim 3 \times 10^{10}\, M_\odot$, as would be the case for galaxies that have had minimal influences from mergers and feedback during their primary star-forming stages.

Along with the GCS catalog itself, we view Figure 14 and the discussion above as the most important result of this paper. The relative number of GCs in a galaxy as measured by either S_N or S_M differs considerably from one system to another, but still follows a systematic trend that can be matched by a single, constant ratio $\eta = M_{\rm GCS}/M_{\rm halo} \simeq 6 \times 10^{-5}$. Our results strongly support recent work (S09; G10) that the GCS is a remarkably simple proxy for the most fundamental characteristic of a galaxy, namely, its dark-matter potential well.

The hypothesis $M_{\rm GCS} \propto M_{\rm halo}$ can explain the basic shape of the S_M distribution with its characteristic rise at extreme low and high luminosities, but it does not address the *scatter* that we see in any given mass range. Quantitatively this scatter is ± 0.25 dex at any point on the mean curve, or slightly less than a factor of two in S_M. We should expect four generic sources of scatter.

1. Random measurement uncertainties in $N_{\rm GC}$ and thus $M_{\rm GCS}$. The raw uncertainties or even the statistical variance in $N_{\rm GC}$, as discussed above, may be up to factors of two depending on the galaxy and are therefore probably the dominant source of the observed scatter.
2. Random uncertainties in the quantities that determine $M_{\rm dyn}$, namely, R_e and σ_e. These behave differently from random scatter in $N_{\rm GC}$, since $S_M \sim M_{\rm GCS}/M_{\rm dyn}$, and thus S_M and $M_{\rm dyn}$ are not independent quantities. Any error in $M_{\rm dyn}$ would generate an equal, inverse change in S_M and would shift points along a diagonal line in Figure 14. If this was, however, an important source of the observed scatter, then it should be most visible at the high-mass end where the S_M curve is nearly perpendicular to that error line. In practice we see rather similar amounts of scatter over a wide range of masses, consistent with the expectation from the raw observations that R_e and σ_e are uncertain to $\lesssim$10% (see Harris et al. 2013).
3. Intrinsic differences in GC formation efficiency between galaxies of similar type and mass. These differences certainly exist (compare the classic well-studied cases of the Virgo giants M87 and M49, which have similar luminosities but GC populations different by almost a factor of three), but it is harder to make any general statements about the amount of such "cosmic scatter" at this stage. A large part of the scatter may be the result of environment: for example, P08 address this question in detail for dwarfs, and find evidence that dE galaxies near dominant giants are more likely to have higher-S_N GCSs. By hypothesis these galaxies may have benefited from being in deeper halo potential wells which increased massive star cluster formation. At the opposite end of the environment scale, Cho et al. (2012) find that E galaxies in very isolated environments have quite low specific frequencies in the range normally associated with spirals or S0s.
4. The stochastic effects of different individual merging and star-forming histories, which are hard to recover in full detail long after the fact, must also play a role in generating galaxy-to-galaxy differences. Conversely, differences in dynamical GC destruction interior to a galaxy should not be a major factor, since internal GC erosion rates should be similar *for galaxies of the same type and luminosity*. Going further into these intriguing questions is beyond the scope of our paper.

Lastly, although some dwarfs and supergiants stand out as having exceptionally high S_M, it is perhaps worth noting as well that many dwarfs and giants have S_M or S_N values that are quite similar to those of the intermediate-luminosity galaxies in the "baseline" middle range. The large size of our new catalog allows this feature of the distribution to stand out more clearly than before. Quantitatively, fully 80% of the *entire* sample in Figure 14 falls within $S_M < 0.3$ (below the dashed line in Figure 14), and 64% fall within $S_M < 0.2$. The median of the whole sample (less sensitive to outliers than the mean) is at $\tilde{S}_M = 0.153$. In terms of specific frequency, 64% of the entire catalog falls below $S_N = 3$ and the median is at $\tilde{S}_N = 2.07$.

It seems that no single starting point for GC formation may work equally well for every galaxy. If GCs form extremely early and the later field-star formation is quenched or disrupted, then the result will be a cluster-rich galaxy. Contrarily, if there is little difference between GC formation times and field-star formation times, then a lower-S_N GC system will result. Therefore, we suggest that the many dwarfs and giants with lower specific frequencies could be ones in which the GC and field-star formation rates versus time were the same as in the intermediate galaxies.

A next step in understanding the link between GC formation and their host galaxies will be to explore more thoroughly the relation with cluster metallicity (color): what does the correlation of S_M versus galaxy mass look like for the red and blue GC subgroups? Another major question is the role of galaxy environment, and how much of the scatter around the S_M and S_N relations is driven by a galaxy's location. Initial work on these questions has started, but extensions to much bigger samples will be valuable.

5. SUMMARY

We summarize the results of our discussion as follows.

1. A new catalog of 422 galaxies with published measurements of their GCSs is presented along with a source bibliography. This list, based on a literature survey to the end of 2012, contains 248 ellipticals (dwarfs and giants), 93 S0s, and 81 spirals and irregulars.
2. Total GC population $N_{\rm GC}$ increases monotonically with either host galaxy luminosity or baryonic mass, but not in a simple linear way. In agreement with other recent studies but now based on a larger sample, we find that the GC specific frequency and specific mass follow a U-shaped trend, with very high S_N at either very low or very high luminosity, but reaching a well-defined mean value $S_N = 1$ and $S_M = 0.1$ in the range $M_{\rm dyn} \sim (2\text{–}3) \times 10^{10}\, M_\odot$. This trend can be understood as the result of the different kinds of feedback operating during galaxy formation: for the low-mass dwarfs, field-star formation is inhibited by radiative feedback, gas ejection, and externally driven damping before it can run to completion; while for giants, early AGN activity and virial heating inhibit field-star formation after the GCs have formed. At intermediate galaxy mass, neither kind of feedback is as important and so these galaxies can form stars the most efficiently. Thus, along with P08 and G10, we identify these minimum S_N, S_M values as the *baseline normal* for star formation minimally damped by feedback or external quenching.
3. High-S_N galaxies such as the extreme dwarfs or supergiants may be ones in which the GC formation epoch preceded the bulk of field-star formation and was therefore less affected by feedback and quenching processes.

4. Previous recent studies including Peng et al. (2008), Spitler et al. (2008), Spitler & Forbes (2009), and Georgiev et al. (2010) have explored the proposal that GC population size (or more importantly, the mass $M_{\rm GCS}$) is directly proportional to the host galaxy halo mass $M_{\rm halo}$. Our work adds support to this interpretation. We find that a single constant ratio $\eta \equiv M_{\rm GCS}/M_{\rm halo} = 6 \times 10^{-5}$ is capable of reproducing the systematic trend of specific mass S_M versus galaxy mass, over the entire range of galaxy sizes and masses. The galaxy-to-galaxy scatter anywhere around this relation is typically a factor of two.
5. We find that GC population size can also be accurately predicted by a simple product of galaxy effective radius and velocity dispersion, as $N_{\rm GC} \sim (R_e\sigma_e)^{1.3}$. The residual scatter is ± 0.32 dex, making it competitive with any other proposed correlation. We show that this relation can be roughly understood from previously known fundamental plane scaling relations among galaxy luminosity, mass, and scale size.

This work makes use of data products from the Two Micron All-Sky Survey, which is a joint project of the University of Massachusetts and the Infrared Processing and Analysis Center/California Institute of Technology, funded by the National Aeronautics and Space Administration and the National Science Foundation. This work was supported in part by the Natural Sciences and Engineering Research Council of Canada through research grants to W.E.H., and by McMaster University through partial summer student salary to M.A. G.L.H.H. wishes to thank ESO/Garching for a visiting scientist fellowship, where the first steps toward building this catalog were carried out. We thank the anonymous referee for suggestions and comments that improved the presentation of this paper.

REFERENCES

Allanson, S. P., Hudson, M. J., Smith, R. J., & Lucey, J. R. 2009, ApJ, 702, 1275
Ashman, K. M., & Zepf, S. E. 1992, ApJ, 384, 50
Baum, W. A. 1955, PASP, 67, 328
Behroozi, P. S., Conroy, C., & Wechsler, R. H. 2010, ApJ, 717, 379
Bezanson, R., van Dokkum, P. G., Franx, M., et al. 2011, ApJ, 737, 31
Bezanson, R., van Dokkum, P. G., Tal, T., et al. 2009, ApJ, 697, 1290
Blakeslee, J. P. 1997, ApJL, 481, L59
Blakeslee, J. P. 1999, AJ, 118, 1506
Bower, R. G., Benson, A. J., Malbon, R., et al. 2006, MNRAS, 370, 645
Brodie, J. P., & Strader, J. 2006, ARA&A, 44, 193
Burgarella, D., Kissler-Patig, M., & Buat, V. 2001, AJ, 121, 2647
Burkert, A., & Tremaine, S. 2010, ApJ, 720, 516
Cappellari, M., Bacon, R., Bureau, M., et al. 2006, MNRAS, 366, 1126
Cho, J., Sharples, R. M., Blakeslee, J. P., et al. 2012, MNRAS, 422, 3591
Dekel, A., & Birnboim, Y. 2006, MNRAS, 368, 2
Dekel, A., & Silk, J. 1986, ApJ, 303, 39
Dekel, A., & Woo, J. 2003, MNRAS, 344, 1131
Djorgovski, S., & Davis, M. 1987, ApJ, 313, 59
Durrell, P. R., Harris, W. E., Geisler, D., & Pudritz, R. E. 1996, AJ, 112, 972
Faber, S. M., Dressler, A., Davies, R. L., Burstein, D., & Lynden-Bell, D. 1987, in Proc. Eighth Santa Cruz Summer Workshop in Astronomy and Astrophysics, Nearly Normal Galaxies, ed. S. M. Faber (New York: Springer), 175
Forte, J. C., Vega, E. I., & Faifer, F. 2009, MNRAS, 397, 1003
Georgiev, I. Y., Goudfrooij, P., Puzia, T. H., & Hilker, M. 2008, AJ, 135, 1858
Georgiev, I. Y., Puzia, T. H., Goudfrooij, P., & Hilker, M. 2010, MNRAS, 406, 1967 (G10)
Georgiev, I. Y., Puzia, T. H., Hilker, M., & Goudfrooij, P. 2009, MNRAS, 392, 879
Graham, A. 2008, PASA, 25, 167
Graves, G. J., & Faber, S. M. 2012, ApJ, 717, 803
Gultekin, K., Richstone, D. O., Gebhardt, K., et al. 2009, ApJ, 698, 198
Hanes, D. A. 1977, MmRAS, 84, 45
Harris, G. L. H., & Harris, W. E. 2011, MNRAS, 410, 2347
Harris, G. L. H., Poole, G. B., & Harris, W. E. 2013, MNRAS, submitted
Harris, H. C., & Harris, W. E. 2000, in Astrophysical Quantities, ed. A. N. Cox (4th ed.; New York: Springer), 545
Harris, W. E. 1991, ARA&A, 29, 543
Harris, W. E. 2001, in Saas-Fee Advanced Course 28, Swiss Society for Astronomy and Astrophysics, ed. L. Labhardt & B. Binggeli (New York: Springer), 223
Harris, W. E. 2009, ApJ, 699, 254
Harris, W. E., & Harris, G. L. H. 2002, AJ, 123, 3108
Harris, W. E., & Racine, R. 1979, ARA&A, 17, 241
Harris, W. E., & Smith, M. G. 1976, ApJ, 207, 1036
Harris, W. E., & van den Bergh, S. 1981, AJ, 86, 1627
Harris, W. E., Whitmore, B. C., Karakla, D., et al. 2006, ApJ, 636, 90
Hopkins, P. F., Hernquist, L., Cox, T. J., Robertson, B., & Krause, E. 2007, ApJ, 669, 67
Hubble, E. 1932, ApJ, 76, 44
Jaschek, C. O. R. 1957, ZA, 44, 23
Jordán, A., McLaughlin, D. E., Côté, P., et al. 2006, ApJL, 651, L25
Jordán, A., McLaughlin, D. E., Côté, P., et al. 2007, ApJS, 171, 101
Jorgensen, I., Franx, M., & Kjaergaard, P. 1996, MNRAS, 280, 167
Kavelaars, J. J. 1999, in ASP Conf. Ser. 182, Galaxy Dynamics, ed. D. R. Merritt, M. Valluri, & J. A. Sellwood (San Francisco, CA: ASP), 437
Kron, G. E., & Mayall, N. U. 1960, AJ, 65, 581
Kundu, A., & Whitmore, B. C. 2001a, AJ, 121, 2950
Kundu, A., & Whitmore, B. C. 2001b, AJ, 122, 1251
Larsen, S. S., Brodie, J. P., Huchra, J. P., Forbes, D. A., & Grillmair, C. J. 2001, AJ, 121, 2974
Leauthaud, A., Tinker, J., Bundy, K., et al. 2012, ApJ, 744, 159
Loeb, A., & Peebles, P. J. E. 2003, ApJ, 589, 29
Lotz, J. M., Miller, B. W., & Ferguson, H. C. 2004, ApJ, 613, 262
Magoulas, C., Springob, C. M., Colless, M., et al. 2012, MNRAS, 427, 245
McConnell, N. J., Ma, C.-P., Murphy, J. D., et al. 2012, ApJ, 756, 179
McElroy, D. B. 1995, ApJS, 100, 105
McLaughlin, D. E. 1999, AJ, 117, 2398
McLaughlin, D. E. 2000, ApJ, 539, 618
McLaughlin, D. E., & Fall, S. M. 2008, ApJ, 679, 1272
McLaughlin, D. E., & van der Marel, R. P. 2005, ApJS, 161, 304
Michard, R. 2005, A&A, 429, 819
Mieske, S., Jordán, A., Côté, P., et al. 2010, ApJ, 710, 1672
Moore, B., Diemand, J., Madau, P., Zemp, M., & Stadel, J. 2006, MNRAS, 368, 563
Novak, G. S., Faber, S. M., & Dekel, A. 2006, ApJ, 637, 96
Papovich, C., Bassett, R., Lotz, J. M., et al. 2012, ApJ, 750, 93
Patel, S. G., van Dokkum, P. G., Franx, M., et al. 2013, ApJ, 766, 15
Peng, E., Jordán, A., Côté, P., et al. 2006, ApJ, 639, 95
Peng, E., Jordán, A., Côté, P., et al. 2008, ApJ, 681, 197 (P08)
Racine, R. 1968, PASP, 80, 326
Rhode, K. L. 2012, AJ, 144, 154
Rhode, K. L., Zepf, S. E., Kundu, A., & Larner, A. 2007, AJ, 134, 1403
Rhode, K. L., Zepf, S. E., & Santos, M. R. 2005, ApJL, 630, L21
Sadoun, R., & Colin, J. 2012, MNRAS, 426, L51A
Sandage, A. R. 1968, ApJL, 152, L149
Shankar, F., Lapi, A., Salucci, P., De Zotti, G., & Danese, L. 2006, ApJ, 643, 14
Shankar, F., Marulli, F., Bernardi, M., et al. 2013, MNRAS, 428, 109
Shapley, H. 1918, ApJ, 48, 154
Snyder, G. F., Hopkins, P. F., & Hernquist, L. 2011, ApJL, 728, L24
Spitler, L. R. 2010, MNRAS, 406, 1125
Spitler, L. R., & Forbes, D. A. 2009, MNRAS, 392, L1 (S09)
Spitler, L. R., Forbes, D. A., Strader, J., Brodie, J. P., & Gallagher, J. S. 2008, MNRAS, 385, 361
Spolaor, M., Kobayashi, C., Forbes, D. A., & Couch, W. 2009, ApJL, 691, L138
Spolaor, M., Proctor, R. N., Forbes, D. A., Couch, W. J., & Hau, G. K. T. 2010, MNRAS, 408, 272
Strom, S. E., Forte, J. C., Harris, W. E., et al. 1981, ApJ, 245, 416
Tiret, O., Salucci, P., Bernardi, M., Maraston, C., & Pforr, J. 2011, MNRAS, 411, 1435
Tortora, C., Napolitano, N. R., Cardone, V. F., et al. 2010, MNRAS, 407, 144
Tremaine, S., Gebhardt, K., Bender, R., et al. 2002, ApJ, 574, 740
Trenti, M., Heggie, D. C., & Hut, P. 2007, MNRAS, 374, 344
van den Bergh, S. 1982, PASP, 94, 459
van den Bergh, S. 2000, PASP, 112, 932
Vesperini, E. 2010, RSPTA, 368, 829
Vetesnik, M. 1962, BAICz, 13, 218
Villegas, D., Jordán, A., Peng, E. W., et al. 2010, ApJ, 717, 603 (V10)
Wolf, J., Martinez, G. D., Bullock, J. S., et al. 2010, MNRAS, 406, 1220
Yang, X., Mo, H. J., & van den Bosch, F. C. 2008, ApJ, 676, 248
Young, M. D., Dowell, J. L., & Rhode, K. L. 2012, AJ, 144, 103